

Direct X-ray Spectral Deprojection of Galaxy Clusters

H. R. Russell^{*}, J. S. Sanders and A. C. Fabian

Institute of Astronomy, Madingley Road, Cambridge CB3 0HA

13 August 2018

ABSTRACT

Temperature, density and abundance profiles of the hot intracluster medium (ICM) are important diagnostics of the complex interactions of gravitational and feedback processes in the cores of galaxy clusters. Deprojection of X-ray data by methods such as PROJCT, which are model dependent, can produce large and unphysical oscillating temperature profiles. Here we validate a deprojection routine, Direct Spectral Deprojection (DSDEPROJ; Sanders & Fabian 2007), showing that it solves some of the issues inherent to model-dependent deprojection routines. DSDEPROJ is a model-independent approach, assuming only spherical symmetry, which subtracts projected spectra from each successive annulus to produce a set of deprojected spectra.

Key words: X-rays: galaxies: clusters — galaxies: clusters: general — intergalactic medium — cooling flows

1 INTRODUCTION

X-ray observations of many low-redshift galaxy clusters find strongly peaked emission in the centre from relatively high density gas with a radiative cooling time below ~ 1 Gyr. Without a compensating source of heat, this gas should cool rapidly causing a drop in the central pressure and a subsequent slow inward flow of the overlying gas known as a cooling flow (Fabian 1994). This cooling flow gas should continue to cool to low temperatures. However, recent high resolution X-ray spectroscopy was unable to find the emission signatures of gas cooling below about ~ 1 keV (Peterson et al. 2003; Kaastra et al. 2004; Peterson & Fabian 2006). In addition, the cool gas masses implied by a cooling flow exceeded the sum of the observed gas masses (eg. Edge & Frayer 2003) and inferred star formation rates by an order of magnitude (Johnstone et al. 1987; Hicks & Mushotzky 2005; Rafferty et al. 2006, O’Dea et al. 2008). A heating mechanism is therefore required to prevent significant amounts of cooling from occurring (see McNamara & Nulsen (2007) for a review).

High spatial resolution images of cluster cores from the *Chandra X-ray Observatory* have revealed huge cavities, shock fronts and cold fronts in the ICM. Cold fronts are sharp boundaries between regions of different temperature and density likely caused by gas sloshing in cluster cores. The X-ray cavities, or bubbles, in the hot gas have been produced by the interaction of jets from the central AGN with the surrounding ICM (eg. Fabian et al. 2003; Forman et al. 2005; Fabian et al. 2006; McNamara & Nulsen 2007). These cavities provide a direct and relatively reliable means of measuring the energy injected by the central radio source. However, whilst AGN heating has been shown to be capable of energet-

ically balancing cooling losses (Birzan et al. 2004; Rafferty et al. 2006; Dunn & Fabian 2006; McNamara et al. 2006), the exact mechanisms by which the energy is transported and dissipated and how the balance is achieved are still unclear.

Structures such as shock fronts and cold fronts provide tools to study the microphysics and transport processes at work in the ICM. These discontinuities allow the measurement of the bulk velocities of the gas in the plane of the sky and the stability of these features provide constraints on thermal conduction, the formation of magnetic draping layers and the strength of hydrodynamic instabilities. Detailed studies of shocks and cold fronts in clusters have shown that transport processes in the ICM can be easily suppressed (Ettori & Fabian 2000; Vikhlinin et al. 2001).

In order to study shocks, cavities and cold fronts in the cluster core, and to relate the properties of cool core gas to the strength of the AGN feedback, we require a reliable method for extracting the core gas properties. A spectrum extracted from the cluster centre on the plane of the sky corresponds to a summed cross-section with a range of spectral components from the core to the cluster outskirts. The spectral properties at any point on the plane of the sky are the emission-weighted superposition of radiation from all points along the line of sight through the cluster. These superimposed contributions from the outer cluster layers can be subtracted off by making an assumption about the line of sight extent, usually assuming the cluster is spherical, and deprojecting the emission to produce deprojected radial profiles in temperature, density and metallicity.

The most commonly used deprojection routine is PROJCT in the X-ray spectral fitting package XSPEC (Arnaud 1996). PROJCT takes spectra from a series of concentric annuli and fits each one with a set of models to account for all the layers of projected emission plus a model for the innermost emitting region. However, PROJCT has been found to be unstable to changes in the radial binning

* E-mail: hrr27@ast.cam.ac.uk

and produce oscillating temperature profiles that do not relate to physical changes in the gas temperature (eg. Fabian et al. 2006). In section 2, we use simulated clusters to show that multiphase gas can be responsible for the unstable PROJCT deprojections.

In section 3, we describe a spectral deprojection routine, DS-DEPROJ and compare the results with PROJCT for simulated clusters. In section 4, we apply both DSDEPROJ and PROJCT to a set of three nearby galaxy clusters which contain shocks, cavities and knots of cool gas in the core. Finally, in section 5, we show that DS-DEPROJ produces stable radial profiles for simulated clusters that have multiple temperature components, sharp breaks in temperature and density or that are extended along the line of sight.

We used XSPEC version 11.3.2 (Arnaud 1996) for all spectral fitting. The MEKAL spectral model (Mewe et al. 1985, 1986; Kaastra 1992; Liedahl et al. 1995) and PROJCT deprojection model used here are the defaults available in that version of XSPEC. Photoelectric absorption was modelled with the PHABS model (Balucinska-Church & McCammon 1992). Abundances were measured assuming the abundance ratios of Anders & Grevesse (1989).

We assume $H_0 = 70 \text{ km s}^{-1} \text{ Mpc}^{-1}$, $\Omega_m = 0.3$ and $\Omega_\Lambda = 0.7$. All errors in fit parameters are 1σ unless otherwise noted.

2 PROJCT

PROJCT fits spectra extracted from a series of concentric annuli simultaneously, to account for each projected component. Each projected spectrum is fitted by one or more components described by a set of parameters, such as temperature and density. Assuming spherical symmetry to calculate suitable geometric factors (Kriss et al. 1983), the projected sum of the components along line of sights are fitted to each spectrum simultaneously. PROJCT reads the inner and outer radii of each annulus from FITS header items to calculate the volume of each corresponding shell.

Johnstone et al. (2005) tested the PROJCT model on synthetic, single-temperature cluster spectra and found that the fitted temperature and density profiles agreed with the true profiles. However, the deprojected temperature profiles generated by PROJCT have been found to oscillate between values separated by several times the uncertainties on the values (eg. for the Perseus cluster, Fabian et al. 2006). This oscillation can disappear if different sized annuli are used, indicating that this is not related to physical changes in the cluster properties. Fabian et al. (2006) suggest that this instability may be caused by multiphase gas or deviation from spherical geometry.

2.1 Simulated Clusters

In order to thoroughly test our deprojection routines, we produced a set of simulated clusters with a range of properties including two-temperature components, sharp breaks in density or temperature and an elongated geometry. The generic simulated cluster was based on a 500ks observation of the Perseus cluster, with redshift $z = 0.0183$ and Galactic absorption $n_{\text{H}} = 0.1 \times 10^{22} \text{ cm}^{-2}$. The radial dependence of the deprojected parameters were given by the analytical approximations:

$$n_e = \frac{3.9 \times 10^{-2}}{(1 + (r/80 \text{ kpc})^2)^{1.8}} + \frac{4.05 \times 10^{-3}}{(1 + (r/280 \text{ kpc})^2)^{0.87}} \text{ cm}^{-3} \quad (1)$$

$$T = \frac{7 \times (1 + (r/100 \text{ kpc})^3)}{(2.3 + (r/100 \text{ kpc})^3)} \text{ keV} \quad (2)$$

$$Z = 0.35 + 0.0139 \left(\frac{r}{\text{kpc}} \right) - 0.000243 \left(\frac{r}{\text{kpc}} \right)^2 + 1.031 \times 10^{-6} \left(\frac{r}{\text{kpc}} \right)^3 Z_\odot \quad \text{for } r < 121 \text{ kpc} \quad (3)$$

$$= 0.3 Z_\odot \quad \text{for } r > 121 \text{ kpc} \quad (4)$$

The radial dependence of the density was determined by Churazov et al. (2003), where the second term, which describes the distribution on larger scales, was taken from Jones & Forman (1999). The expression for the gas temperature distribution was also taken from Churazov et al. (2003). An approximate fit to the observed abundance profile of the Perseus cluster was used for the abundance distribution.

The FAKEIT command and a PHABS(MEKAL+MEKAL) model in XSPEC were used to create artificial spectra for the two-temperature galaxy cluster with the parameters set according to the supplied equations and then folded through suitable response files. The input parameters for the second MEKAL component were also determined by equations 1–4, but the temperature and density at each radius were halved. The projected spectra were generated by stepping through the cluster radius on the sky and, for each radius, summing all the artificial spectra along the line of sight. The final simulated projected spectra were grouped into bins with a minimum of 50 counts, allowing the use of χ^2 statistics.

This same simulated dataset was used throughout sections 2 and 3 to allow a consistent interpretation of the deprojection methods. The enhanced metallicity in the second annulus from the centre, which for these noisy core spectra results in lower temperature and density best-fitting values, and the fluctuations in the profiles from 50 – 100kpc are particular to this simulated cluster (eg. Figure 3). Deprojections of other simulated clusters do not also display these specific features.

2.2 Single-temperature Model

We fitted these two-temperature synthetic spectra with an absorbed single-temperature MEKAL thermal model and PROJCT in XSPEC 11.3.2. The redshift and Galactic hydrogen column density were fixed to the simulated cluster values $z = 0.0183$ and $n_{\text{H}} = 0.1 \times 10^{22} \text{ cm}^{-2}$. The temperature, metallicity and model normalization (relating to density) parameters were allowed to vary and the resulting profiles are shown overlaid on the true profiles in Figure 1. The single-temperature PROJCT profile appears to bounce between the two temperature components suggesting that PROJCT tends to account for one temperature component in one shell and the other component in a neighbouring shell. If we assume that the single-temperature spectral model is a good fit to the data, a very misleading result is produced.

As an aside, we note that the bounce in the outermost annulus of the density profile (Figure 1) is caused by a different effect. The emission extends beyond the outermost annulus of each cluster we analysed so that the emitting volume associated with this annulus is too small. This causes an overestimate of the projection on to the next annulus in, so that the fit to that annulus underestimates its brightness. However, the effect is minimal for the annuli beyond the outer two because the steep surface brightness profile limits the amount of projection.

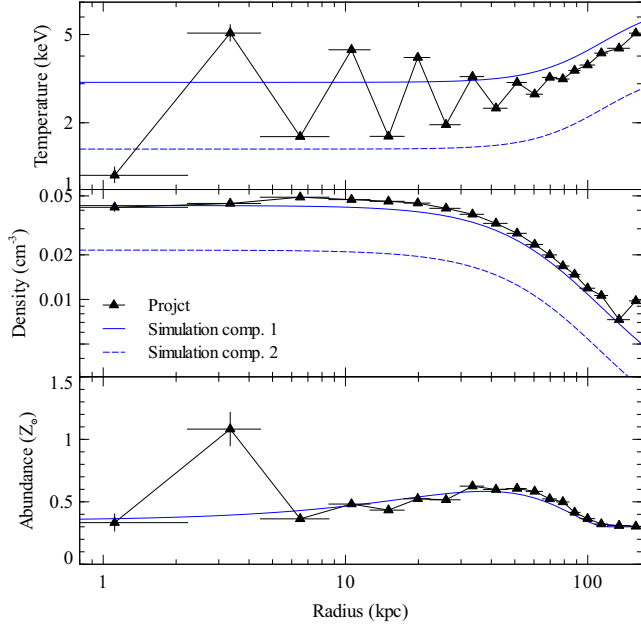


Figure 1. Deprojected temperature (top), electron density (centre) and metallicity (bottom) profiles for a two-temperature simulated cluster. The single-temperature PROJCT fit to the data is overlaid on the true profiles.

2.3 Fixing Parameters in PROJCT

The oscillation in the temperature profile can sometimes be alleviated by fitting the annuli sequentially from the outside and freezing the parameters of components in the outer shells before fitting spectra from shells inside them (PROJCTFIXED; see eg. Sanders et al. 2004). This prevents the poorly modelled spectra near the centre from affecting the results in outer annuli. However, this method underestimates the uncertainties on the model parameters because the outer shell uncertainties are not included. Figure 2 shows that freezing the outer shell parameters does remove some of the oscillation in the outer shells but that this approach produces particularly poor fits for the innermost annuli.

2.4 Two-temperature Model

A two-temperature MEKAL model can be fitted to the data if there are sufficient counts to produce well-constrained parameters. We reduced the number of free model parameters in each annulus by tying the abundance parameters together, leaving the two temperature parameters and the normalizations free. The redshift and Galactic hydrogen column density were fixed to the simulated cluster values $z = 0.0183$ and $n_{\text{H}} = 0.1 \times 10^{22} \text{ cm}^{-2}$.

Figure 3 shows that a two-temperature model provides a much better fit to the simulated profiles with $\chi^2_{\nu} = 1.00$ compared to $\chi^2_{\nu} = 4.56$ for the single-component model. The two-temperature model closely follows the true cluster profiles except for the two innermost annuli. The spectra from the inner annuli contain a large quantity of projected emission which, when subtracted off, leaves particularly noisy deprojected spectra for those shells.

In summary, we have shown that assuming a single-component PROJCT model for a cluster with two spectral components, produces an oscillating temperature profile with values that are unrelated to physical changes in the cluster gas. Similar deprojection methods which assume a spectral model for the deprojec-

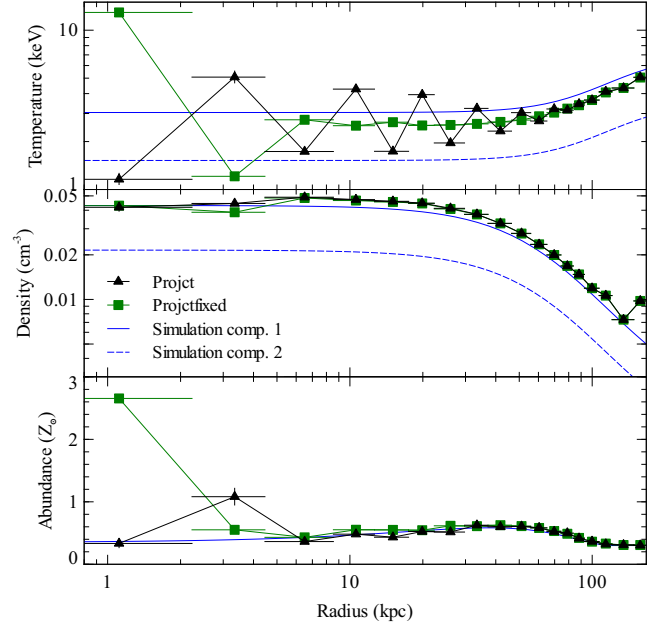


Figure 2. Deprojected temperature (top), electron density (centre) and metallicity (bottom) profiles for a two-temperature simulated cluster. The standard single-temperature PROJCT fit and the single-temperature PROJCTFIXED fit are overlaid on the true cluster profiles. There are no vertical error bars for the PROJCTFIXED model (green line)

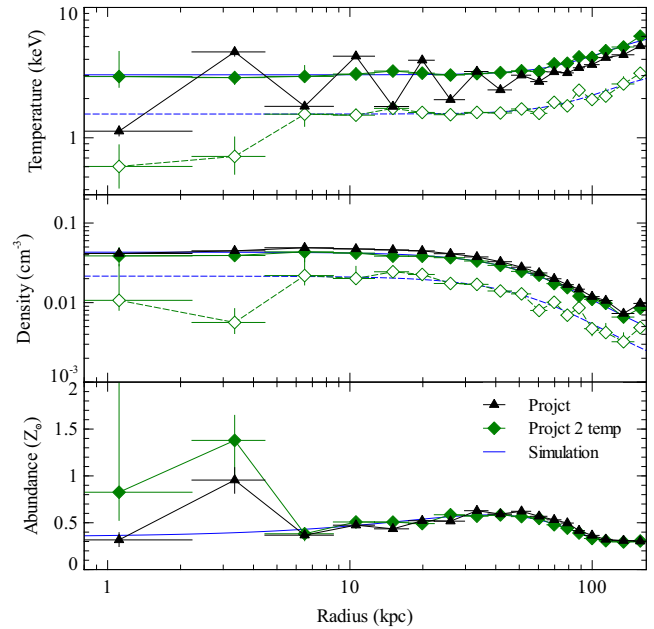


Figure 3. Deprojected temperature (top), electron density (centre) and metallicity (bottom) profiles for a two-temperature simulated cluster with lines indicating the two spectral components of the true cluster (solid and dashed blue), single-temperature PROJCT fit (black triangles), two-temperature PROJCT fit (solid and open green diamonds).

tion will suffer from the same problem. To provide a solution to this issue, we present and validate a new deprojection routine, DSDEPROJ, which assumes only spherical geometry.

3 DSDEPROJ

DSDEPROJ (Sanders & Fabian 2007) is a model-independent deprojection method which, assuming only spherical symmetry, uses a purely geometrical procedure to subtract off the projected emission in a series of shells (similar to Nulsen & Bohringer 1995). The resulting deprojected spectra can then be fitted with single or multiple temperature models in XSPEC to produce deprojected profiles in temperature, density and metallicity.

DSDEPROJ takes as inputs: spectra extracted from a series of concentric annuli in a sector of the cluster and suitable blank-sky backgrounds. DSDEPROJ then performs the following steps:

- (i) Subtract the equivalent background spectrum from each of the foreground cluster spectra
- (ii) Start at the spectrum from the outermost annulus: divide the count rate in each spectral energy bin by the emitting volume, assuming it was emitted from a section of a spherical shell, (geometric factors from Kriss et al. 1983) to give a spectrum per unit volume
- (iii) Scale the spectrum per unit volume from the outermost annulus by the volume projected onto the neighbouring inner annulus, and subtract this from the count rate in each spectral bin of that annulus
- (iv) Calculate a new count rate per unit volume in each spectral bin for this inner shell
- (v) By moving inwards to each successive annulus, we can subtract off the projected emission of each outer shell from the inner shells and produce a set of deprojected spectra

We used a Monte Carlo technique to calculate the uncertainties in the count rate of each spectral channel in each spectrum. Each of the input foreground cluster and background spectra are binned to have 200 counts per spectral channel so that Gaussian errors can be assumed. The deprojection process is repeated 6000 times, each time creating new input foreground cluster and background spectra by simulating spectra drawn from Gaussian distributions based on the initial spectra and their uncertainties. The output spectra are the median output spectra calculated in this process. The 1σ errors on the count rates in each spectral channel are calculated from the 15.85 and 84.15 percentile spectra.

3.1 Single-temperature Model

Figure 4 shows the deprojection of the two-temperature simulated cluster spectra with DSDEPROJ and the previous result from PROJCT. DSDEPROJ produces a smooth temperature profile that is the average of the two separate components (weighted by emission). The errors in the parameters increase towards the cluster centre as each subsequent annulus has an increasing amount of projected emission which must be subtracted off. This is particularly apparent for the central two radial bins.

3.2 Two-temperature Model

The deprojected spectra produced by DSDEPROJ were also fitted with an absorbed two-temperature MEKAL model to check that the two components of the simulated cluster are correctly reproduced

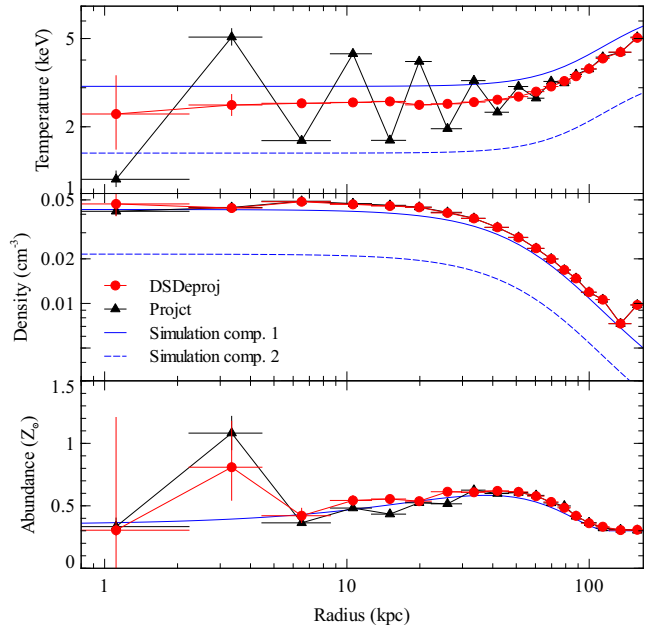


Figure 4. Deprojected temperature (top), electron density (centre) and metallicity (bottom) profiles for a two-temperature simulated cluster. The single-temperature PROJCT and DSDEPROJ results are overlaid on the true cluster profiles.

(Figure 5). We compared the result with that of PROJCT by leaving the two temperature parameters and the normalization free and tying the abundance parameters for the two components together. The redshift and Galactic hydrogen column density were fixed to the simulated cluster values $z = 0.0183$ and $n_H = 0.1 \times 10^{22} \text{ cm}^{-2}$. We found that both DSDEPROJ and PROJCT recovered the simulated cluster profiles with a two temperature spectral model.

A detailed validation of the DSDEPROJ routine for a series of simulated clusters is given in section 5.

4 DEPROJECTION OF A SAMPLE OF GALAXY CLUSTERS

We applied DSDEPROJ and PROJCT to *Chandra* archive observations of three nearby ($z < 0.1$) galaxy clusters: Perseus, Hydra A and Abell 262. These clusters each have deep archive observations with total exposure times of 890ks, 200ks and 110ks, respectively. Deep observations of nearby bright clusters yield a large number of counts for each cluster which ensures a detailed deprojection with a large number of fine bins and a significant detection of multiple temperature components.

4.1 Data Reduction

The data were analysed using CIAO version 4.0 beta 2 with CALDB version 3.4.1 provided by the *Chandra* X-ray Center (CXC). The level 1 event files were reprocessed to apply the latest gain and charge transfer inefficiency correction and then filtered for bad grades. The improved background screening provided by VFaint mode was applied where available. The background light curves of the resulting level 2 events files were filtered to remove periods affected by flares using the CIAO script LC_CLEAN. Background spectra were extracted from the blank-sky background data

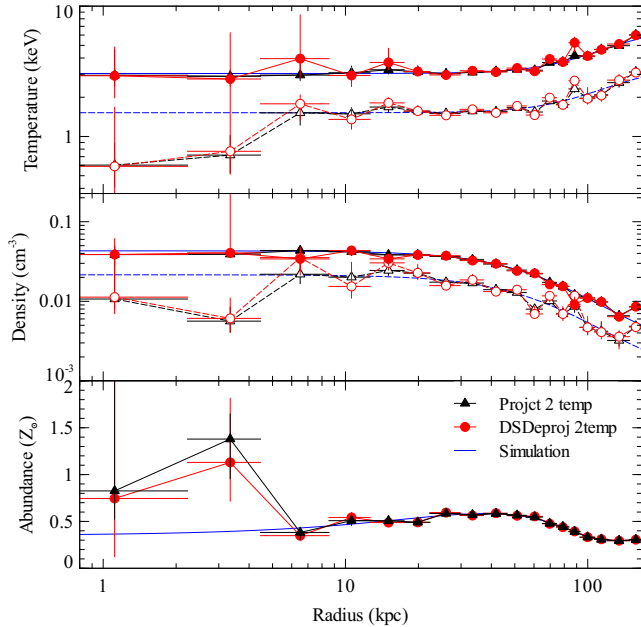


Figure 5. Deprojected temperature (top), electron density (centre) and metallicity (bottom) profiles for a two-temperature simulated cluster. The two-temperature PROJCT (black solid and open triangles) and DSDEPROJ results (red solid and open circles) are overlaid on the true cluster profiles (blue solid and dashed lines).

sets available from the CXC and cleaned using the same method applied to the cluster observations. These background spectra were normalized so that the count rate of the source and background observations matched in the 9 – 12 keV band.

For each cluster, we identified a suitable sector for deprojection and extracted a series of spectra in concentric annuli centred on the surface brightness peak. In the Perseus cluster we selected a sector containing the weak shock analysed in Graham et al. (2008). For Abell 262 we defined a sector which enclosed the half of the cluster where the X-ray emission was most extended. Spectra from Hydra A were extracted from complete annuli. Individual sources were identified using the WAVDETECT algorithm in CIAO. Sources were visually confirmed on the X-ray image and excluded from the analysis.

Each cluster sector was divided up into a series of annuli to give a minimum of 3000 counts in each deprojected spectrum. This criterion provides enough deprojected counts to allow a good spectral fit and measurement of the temperature, density and abundance in each shell. All spectra were analysed in the energy range 0.5 – 7 keV using XSPEC version 11.3.2 and grouped with a minimum of 50 counts per spectral bin. Response and ancillary response files were generated for each cluster spectrum, weighted according to the number of counts between 0.5 and 7 keV. The cluster spectra were then deprojected with DSDEPROJ and PROJCT in XSPEC. In addition, we fitted the annuli in series using the PROJCT model with the parameters in the outer annuli fixed to their best fit values (see Section 2).

For the single-temperature deprojections, an absorbed plasma MEKAL model was fitted to each spectrum in XSPEC. The redshift was fixed to the values given in Table 1 and the absorbing column density was fixed to the Galactic values given by Kalberla et al. (2005). The temperature, metallicity and model normalization were allowed to vary.

The PROJCT two-component model fitted to these real clusters was not readily able to find a minimum. The large number of parameters meant that the fit was poorly constrained and unable to converge on a solution. We exclude this model from our analysis of the cluster sample. The two-temperature DSDEPROJ model also produced poorly constrained parameters when fitted to the cluster sample. The use of this model was restricted to the Perseus cluster, for which the best quality data is available. We used a set of 20 annuli with a minimum of 190,000 counts per annulus to produce deprojected spectra which could constrain a two-temperature fit in each shell.

4.2 The Perseus cluster

The data used for this analysis were first presented in the deep study of the Perseus cluster (Abell 426) in Fabian et al. (2006). The total good exposure time from the combined *Chandra* observations is 890 ks. This deep observation has revealed details of the complex interaction between the central AGN and the surrounding ICM. Depressions or cavities in the X-ray correspond to bubbles of relativistic plasma that have been inflated by jets from the nucleus and displaced the surrounding gas (Boehringer et al. 1993; Fabian et al. 2000). The outer bubbles are presumably from past activity, having detached from the nucleus and risen buoyantly outwards through the cluster core. Shocks and cool gas around the inner bubbles and ripples in the surrounding gas, interpreted as sound waves, also provide a challenge for any deprojection routine.

For our deprojection analysis we focused on a sector of the cluster core containing a section of the weak shock that surrounds the inner bubbles (Figure 6; Graham et al. 2008). Spectra were extracted from a series of 20 radial bins in this sector spaced 0.1 arcmin in radius. In an analysis of a similar region, Fabian et al. (2006) found the deprojected temperatures produced by PROJCT to be unstable depending on which radial bins were used. They concluded that this may be due to non-spherical geometry or a multiphase gas.

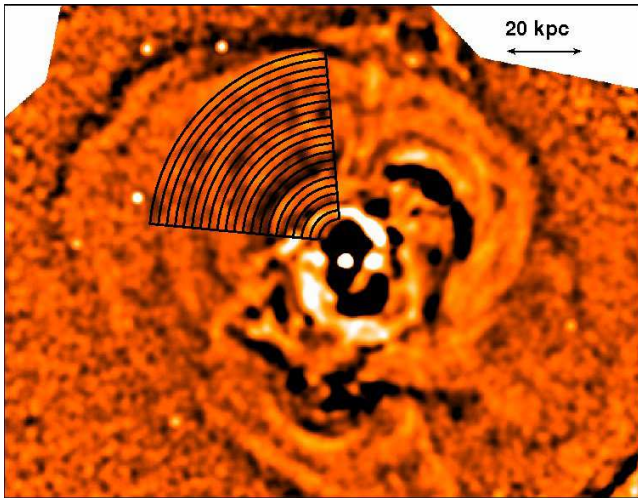
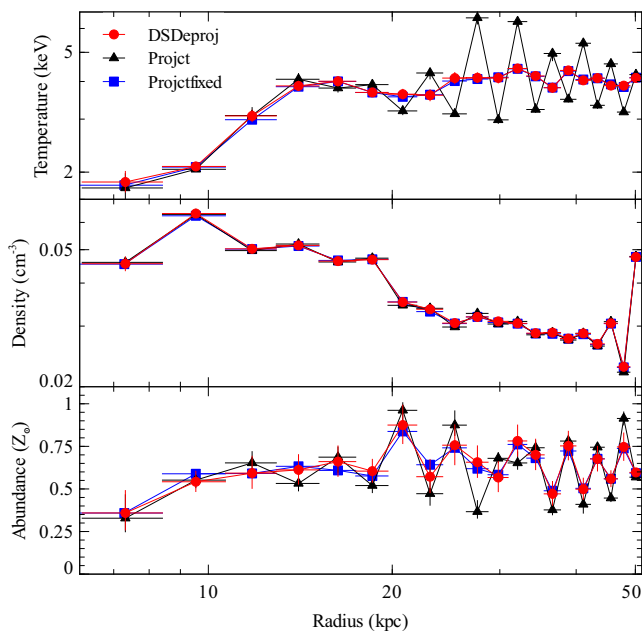
Sanders & Fabian (2007) found significant variations in the model absorption parameter, n_{H} , across the image of the Perseus cluster. Most of this variation is likely due to the cluster’s proximity to the Galactic plane. Leaving the n_{H} parameter free for the spectral fits in this analysis did not produce any significant differences in the radial profiles.

Figure 7 shows the results of the deprojection routines with single-temperature spectral models applied to the sector of the Perseus cluster. In agreement with Fabian et al. (2006), we found that PROJCT produced an unstable deprojected temperature profile with temperatures depending on the positioning of the radial bins. This oscillation, from ~ 20 – 50 kpc in the top panel of Figure 7, is caused by the multiphase gas in the Perseus cluster core. DSDEPROJ produced a smooth temperature profile, revealing a decline in temperature from ~ 4 keV to below 2 keV. PROJCTFIXED produced similar deprojected profiles although this method does not correctly calculate errors on the parameters.

PROJCT and DSDEPROJ produced similar stable deprojected density profiles (middle panel of Figure 7). The sharp increase in density in the outermost radial bin for all three methods shows that there is still a significant amount of projected emission in that bin. The outer two bins should therefore be excluded from any quantitative analysis. The two annuli around 11 kpc show a drop in both the temperature and density, corresponding to a drop in the thermal pressure of the gas. There is also a jump in the density at 20 kpc

Table 1. *Chandra* observations included in this analysis.

Cluster	Obs. ID	Aim Point	ACIS Mode	Total Exposure (ks)	z	n_{H}^1
Abell 262	7921	ACIS-S	VFAINT	110	0.0166	0.0567
Hydra A	4969, 4970	ACIS-S	VFAINT	200	0.0549	0.0468
Perseus	3209, 4289, 4946, 4947, 4948, 4949, 4950, 4951, 4952, 4953, 6139, 6145, 6146	ACIS-S	FAINT	890	0.0183	0.132

¹Galactic absorption column density (in units of 10^{22} cm^{-2}) adopted in this paper (Kalberla et al. 2005).**Figure 6.** Unsharp mask image of the Perseus cluster made from the 0.3 – 7 keV band by subtracting an image smoothed with a Gaussian of width 10 arcsec from one smoothed by 2.5 arcsec and dividing by the sum of the two images. The annuli used for deprojection have been overlaid in black.**Figure 7.** Deprojected temperature (top), electron density (centre) and metallicity (bottom) profiles for the Perseus cluster. There are no vertical error bars for the PROJECTFIXED model (blue line).

which is associated with the weak shock. These features are discussed in more detail by Graham et al. (2008).

Although the metallicity is not as well-constrained as the density or temperature, the fluctuations in the radial profile were found to be stable for different radial binning. The structure in the metallicity profile likely relates to real blobs of high or low metallicity in the ICM (see Sanders & Fabian (2007) for detailed metallicity maps).

A multi-component fit to the DSDEPROJ deprojected spectra was only possible for the high quality spectra from the Perseus cluster. Each of the deprojected spectra were fitted with a variable number of thermal components, using an F-test to ensure that the addition of each one was statistically significant. An F-test probability of less than 0.1 was required for an extra model component to be added. For each component, the Galactic absorption and redshift were fixed to the values in Table 1 and the abundance parameters were tied together. The temperature, model normalization and abundance parameters were allowed to vary.

Half of the radial bins required an extra thermal component at either a lower temperature of 0.5 – 1 keV or a much higher temperature component of > 10 keV. The northern edge of the sector includes a section of the filamentary structures seen in the soft X-ray (Fabian et al. 2003). These filaments have been found to correlate with detections of cool gas in $\text{H}\alpha$ (Conselice et al. 2001) and CO (Salomé et al. 2006). Each of the deprojected annuli likely contains a component of this cool gas but in differing proportions.

We found that the higher temperature component could be equally as well fitted by a power-law component with a photon index $\Gamma \sim 1.5$. Sanders et al. (2004) found evidence for a distributed hard emission component surrounding the core of the Perseus cluster by fitting a high-temperature thermal component. If the origin is hot thermal gas, this material could be from a shock caused by a merger with the nearby high velocity system (Sanders & Fabian 2007).

4.3 Abell 262

The inner regions of Abell 262 also host complex structures, including bright knots of emission and a clear cavity to the east of the cluster centre which is coincident with a lobe of radio emission (Blanton et al. 2004). Blanton et al. (2004) found that the knots of structure in the core are located in the same region as optical [N II] line emission, suggesting that the gas is cooling down to temperatures of $\sim 10^4$ K in these regions.

For a deprojection analysis, we selected a sector of the cluster that covers the extended region of emission to the south of the nucleus and avoids the ~ 5 kpc diameter bubble cavity (Figure 8). The effect of cavities on the deprojection was examined in detail for Hydra A, which has a much more complex system of bubbles. For Abell 262, we focused on the effect of the cool knots of emission.

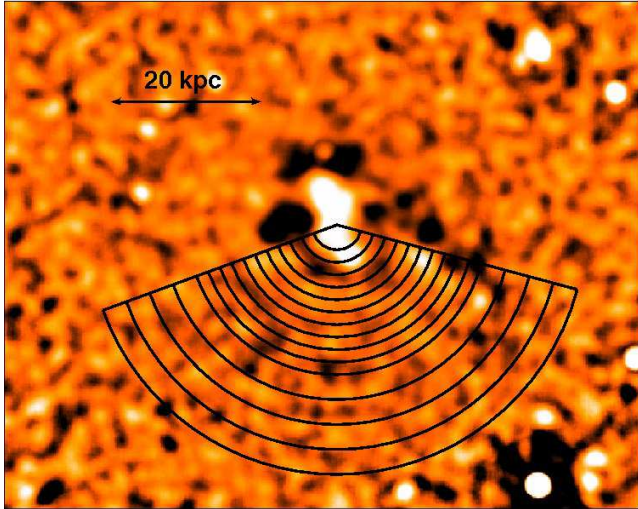


Figure 8. Unsharp mask image of Abell 262 made from the 0.3 – 7 keV band by subtracting an image smoothed with a Gaussian of width 10 arcsec from one smoothed by 2.5 arcsec and dividing by the sum of the two images. The annuli used for deprojection have been overlaid in black.

The single-temperature deprojection of this sector is shown in Figure 9. PROJCT generated an oscillating temperature profile and a sharp discontinuity in the density and abundance at 6 kpc. This is the only cluster in our sample for which PROJCT produced spurious results in all three parameter profiles. The discontinuity at 6 kpc coincides with the edge of the dense core and the jump at ~ 13 kpc may correspond to a bright knot of emission at the northern edge of the sector (Figure 8).

The sharp drop in the density parameter was caused by the unphysically large value of the metallicity; the spectrum was dominated by line emission with only a minimal amount of continuum. We attempted to solve this problem by placing constraints on the metallicity parameter. The PROJCT deprojection was repeated with the metallicity parameter in the third annulus, centred on ~ 6 kpc, fixed to $1Z_{\odot}$. However, this merely pushed the discontinuity into a nearby annulus. Imposing an upper limit of twice solar on the metallicity parameter in each annulus (Johnstone et al. 2005) reduced the drop in density in the third annulus, although this was still inconsistent with DSDEPROJ and the metallicity parameter reached the allowed maximum of twice solar in seven annuli. The constraints on metallicity still produced oscillating temperature profiles.

DSDEPROJ produced a steady decline in temperature and a smooth density profile with a steeper gradient around 6 kpc indicating the edge of the dense core. We tested for the significance of a second temperature component in the annulus centred on 6 kpc by fitting the deprojected spectrum with a two-temperature model. Although the density and abundance parameters were poorly constrained in this model, the F-test probability indicated that the addition of a second component at a temperature of $0.79^{+0.07}_{-0.06}$ keV significantly improved the fit.

4.4 Hydra A

Hydra A (Abell 780) was observed by *Chandra* for two pointings of 100 ks in ACIS-S (ObsID 4969 and 4970). Spectra were extracted from complete annuli in both observations, deprojected and fitted

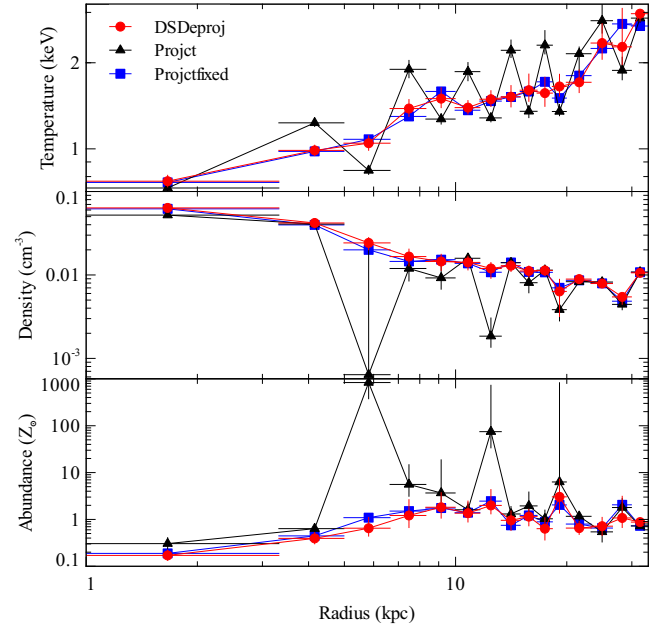


Figure 9. Deprojected temperature (top), electron density (centre) and metallicity (bottom) profiles for Abell 262. There are no vertical error bars for the PROJCTFIXED model (blue line).

together in XSPEC. The central 1.5 arcsec of the cluster, containing the AGN, was excluded from the regions analysed (Figure 10).

The large-scale X-ray morphology of this cluster is generally smooth, however the core reveals the presence of cavities in the ambient cluster gas caused by outbursts from the central AGN (McNamara et al. 2000; David et al. 2001; Nulsen et al. 2002; Nulsen et al. 2005; Wise et al. 2007). These bubbles in the ICM are coincident with radio lobes from the central FR type I radio source 3C 218 (McNamara et al. 2000). Nulsen et al. (2002) found that cooler gas extends outward from the centre of the cluster, beyond the cavities, in the direction of the radio source axis. There will therefore be significant quantities of cooler gas in each deprojected annulus.

The single-temperature deprojection of Hydra A is shown in Figure 11. The PROJCT temperature profile for this cluster is particularly unstable with large oscillations in the temperature parameter throughout the core. Although the DSDEPROJ result also appears to oscillate, the errors are consistent with a smooth temperature profile for the inner radial bins. The density profiles show a smooth increase towards the centre of the cluster with no features that can be readily associated with the large system of cavities in the X-ray emission. The effects of this structure were averaged out when using complete annuli. The metallicity profile was approximately consistent with a constant value of $\sim 0.5Z_{\odot}$.

Two sectors of Hydra A, one containing the northern set of cavities and the second about a perpendicular axis, were separately deprojected but we were unable to significantly detect the inner X-ray cavities in the former.

5 DSDEPROJ VALIDATION

Multiphase gas in observed clusters is not evenly distributed but tends to be concentrated in cluster cores and, in addition, the ICM contains sharp features such as shocks and cold fronts. We have

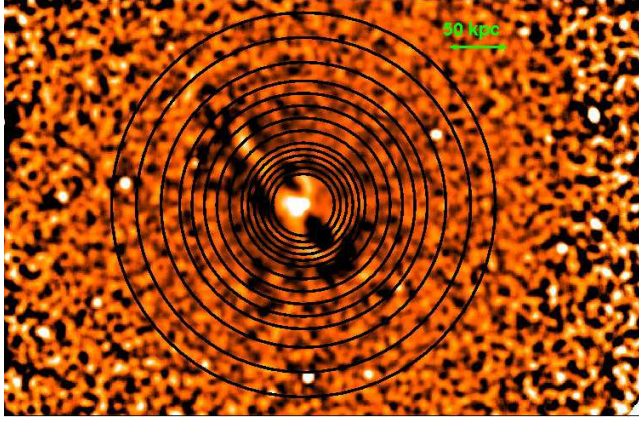


Figure 10. Unsharp mask image of Hydra A made from the 0.3 – 7 keV band by subtracting an image smoothed with a Gaussian of width 10 arcsec from one smoothed by 2.5 arcsec and dividing by the sum of the two images. The annuli used for deprojection have been overlaid in black, excluding the inner 9 annuli which are very finely spaced. The innermost black circle corresponds to a radius of 26 kpc.

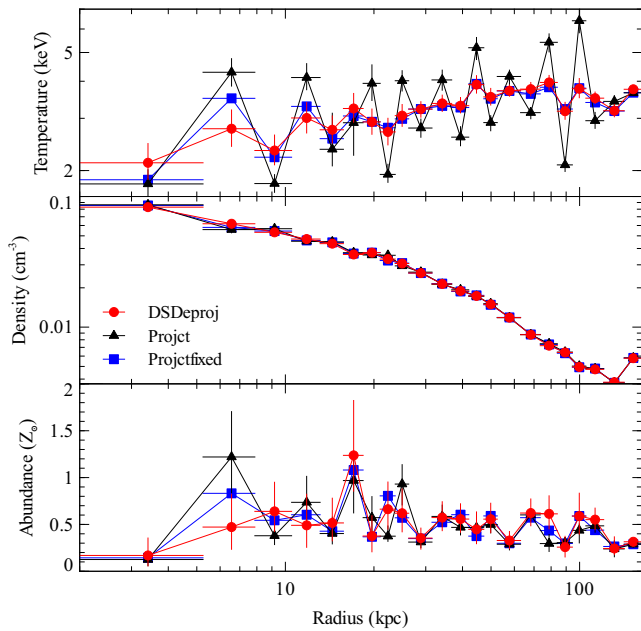


Figure 11. Deprojected temperature (top), electron density (centre) and metallicity (bottom) profiles for Hydra A. There are no vertical error bars for the PROJECTFIXED model (blue line).

tested DSDEPROJ on a variety of simulated clusters containing examples of these features to check that the expected result was recovered.

DSDEPROJ calculates deprojected profiles that are stable for almost any choice of radial binning. Figure 12 shows the DSDEPROJ deprojection of a simulated galaxy cluster under two different radial bin distributions. The two DSDEPROJ deprojections produce profiles that are consistent and stable. As we show later, instabilities only occur when a radial bin contains drastically different gas properties, such as both sides of shock. For comparison, we show the equivalent result under a deprojection with PROJECT in Figure 13.

In section 3, we use a simulated cluster based on the Perseus

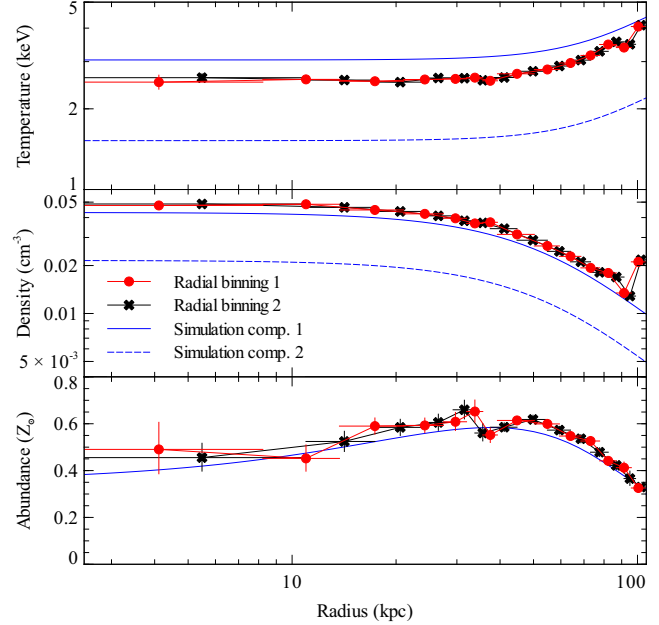


Figure 12. Deprojected temperature (top), electron density (centre) and metallicity (bottom) profiles for a two-temperature simulated cluster. The single-temperature DSDEPROJ results for two different radial bin distributions are overlaid on the true cluster profiles.

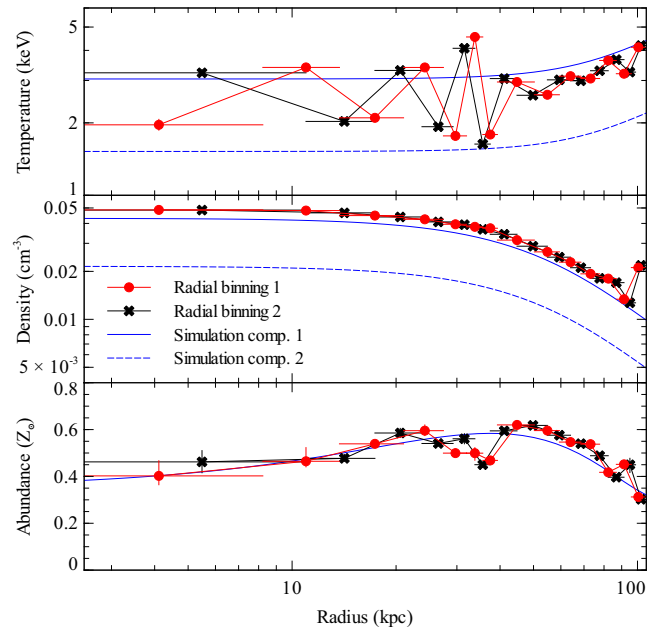


Figure 13. Deprojected temperature (top), electron density (centre) and metallicity (bottom) profiles for a two-temperature simulated cluster. The single-temperature PROJECT results for two different radial bin distributions are overlaid on the true cluster profiles.

cluster to show that DSDEPROJ produces smooth, stable temperature profiles which accurately reproduce the simulated profile. The density and temperature profiles for these simulated clusters are particularly flat in the radial region considered so we also tested DSDEPROJ on simulated clusters with steep power-law profiles in temperature and density given by the equations

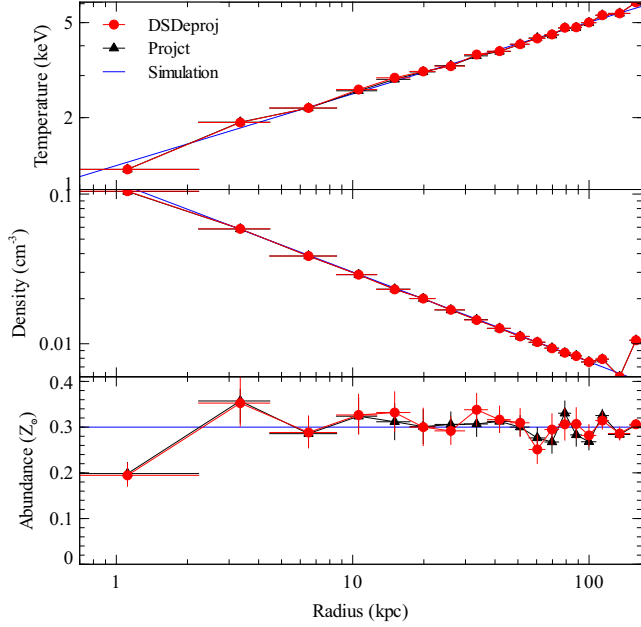


Figure 14. Deprojected temperature (top), electron density (centre) and metallicity (bottom) profiles for a single-temperature simulated cluster with a steep power-law density profile.

$$\begin{aligned}
 T &= 1.26r^{0.3} \text{ keV} \\
 &= 12 \text{ keV} \quad \text{for } r > 2 \text{ Mpc}
 \end{aligned}
 \quad (5)$$

$$n_e = 0.12 \left(\frac{r^{-0.6}}{\text{kpc}} \right) \text{ cm}^{-3} \quad (6)$$

$$Z = 0.3 Z_{\odot} \quad (7)$$

where r is the cluster radius in units of kpc. Both DSDEPROJ and PROJCT correctly reproduce the steep temperature drop and density profile (Figure 14).

We tested the assumption of spherical symmetry by applying DSDEPROJ to a cluster that was stretched by a third along the line of sight (Figure 15). DSDEPROJ and PROJCT correctly reproduce the expected profiles; the central radial bin is poorly constrained because the spectrum contains residuals from the incorrect subtraction of the outer layers. Assuming incorrect cluster geometry does not produce oscillating profiles in PROJCT (or DSDEPROJ), however DSDEPROJ could be modified for the deprojection of non-spherical systems.

We also constructed clusters with a sharp drop or rise in temperature or density at a particular radius. Figure 16 shows the deprojected profiles of a cluster with a temperature break at 42 kpc. DSDEPROJ and PROJCT both reproduce the breaks in temperature without any additional oscillation in the deprojected profile. However sharp changes in density can cause additional ringing in the density and temperature profiles (dashed lines in Figure 17). The density parameter in the shell containing the density break cannot account for the two distinct values causing an under- or overestimation of the projection onto the next shell. This problem can be alleviated by shifting the radial bins so that the density jump occurs close to the edge of a bin (solid lines in Figure 17).

As a final note, DSDEPROJ assumes that the response of the de-

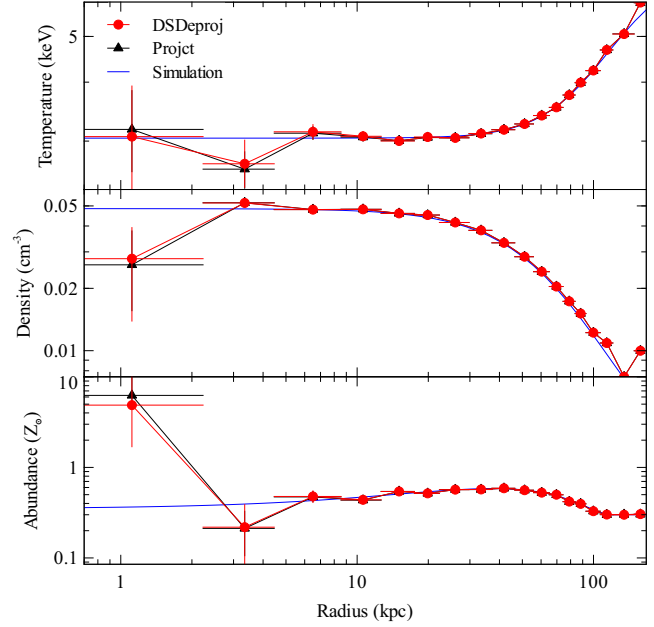


Figure 15. Deprojected temperature (top), electron density (centre) and metallicity (bottom) profiles for a single-temperature simulated cluster which is elongated along the line of sight.

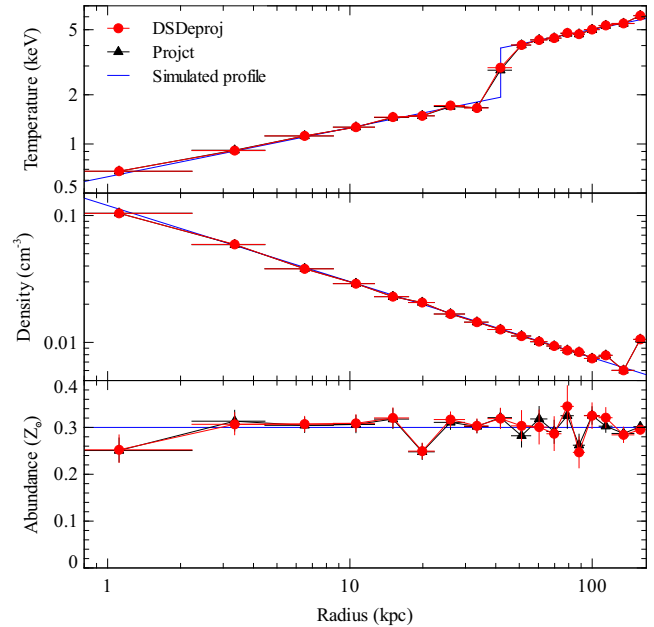


Figure 16. Deprojected temperature (top), electron density (centre) and metallicity (bottom) profiles for a single-temperature simulated cluster which has a sharp temperature break.

tektor does not vary significantly, which is the case for the *Chandra* ACIS-S3 used in this work. An additional routine which uses the ancillary response files to correct for changes in the effective area has been incorporated into DSDEPROJ, however this is not required here. For the ACIS-S3 detector any variation in effective area has a negligible effect on the deprojection (Figure 18).

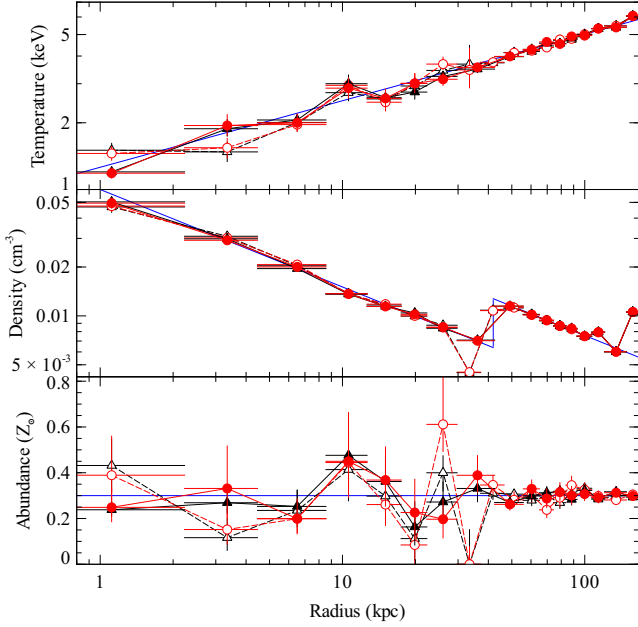


Figure 17. Deprojected temperature (top), electron density (centre) and metallicity (bottom) profiles for a single-temperature simulated cluster which has a sharp density break. The true cluster profile is shown by the blue line; the DSDEPROJ and PROJCT deprojected profiles are shown by red circles and black triangles respectively. The open points with dashed lines indicate a deprojection where the density jump was positioned in the centre of a radial bin; solid points and lines denote the deprojection with the density jump shifted to the edge of the radial bin.

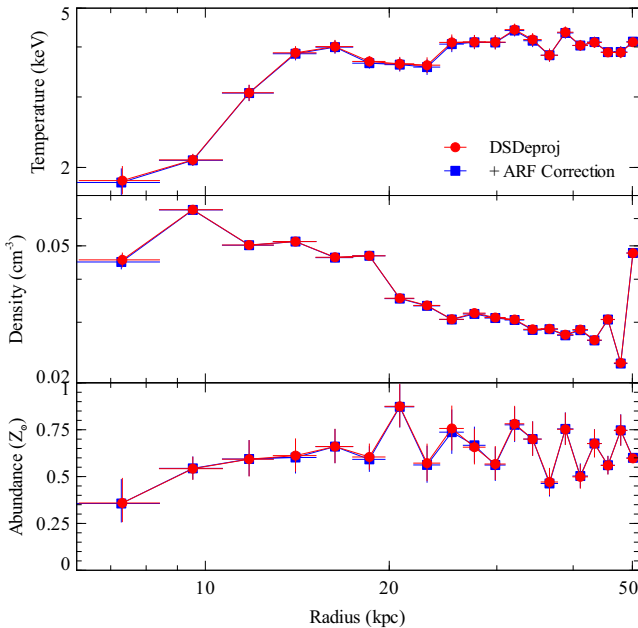


Figure 18. Deprojected temperature (top), electron density (centre) and metallicity (bottom) profiles for the Perseus cluster. The deprojected profiles were created with (blue line) and without (red line) an ancillary response correction to illustrate that there is no significant difference.

6 SUMMARY

We have investigated several issues regarding the reliable deprojection of galaxy clusters and validated the deprojection routine DSDEPROJ. Deprojection methods that assume a spectral model for the deprojection, such as PROJCT in XSPEC, have previously been found to produce temperature profiles which bounce between unphysical values separated by several times their uncertainty. We have shown that this effect is caused by fitting multiphase gas with a single-temperature model. Although a two-temperature PROJCT deprojection recovers the true profiles for the simulated clusters, the majority of the cluster observations currently available in the *Chandra* archive do not have a sufficient number of counts to constrain the two-components in a detailed deprojection.

DSDEPROJ, our deprojection routine which assumes only spherical geometry, solves some of these issues inherent to model-dependent deprojection routines. DSDEPROJ produces a set of ‘deprojected spectra’ which can then be fitted by a suitable spectral model in XSPEC. We have shown that this method does not generate the oscillating temperature profiles for multi-temperature clusters and produces a stable solution for an elongated cluster and clusters with breaks in temperature or density.

PROJCT and DSDEPROJ were applied to a small sample of three nearby galaxy clusters, each of which has a component of cooler gas or complex substructure in the core. PROJCT produced a rapidly oscillating temperature profile for each cluster and, in Abell 262, unphysical values of density and abundance. The deprojected profiles generated by DSDEPROJ were smoothly varying, producing stable solutions at shocks, knots of substructure and with different radial binning. DSDEPROJ was only able to constrain a two-temperature spectral model for the Perseus cluster deprojection. This revealed a low temperature component in several annuli that contain cool gas filaments and a power-law component associated with a distributed hard emission component (Sanders et al. 2004).

The DSDEPROJ source code is available at www.xray.ast.cam.ac.uk/papers/dsdeproj

ACKNOWLEDGMENTS

HRR and ACF acknowledge support from the Science and Technology Facilities Council and the Royal Society, respectively. We thank the referee for helpful comments.

REFERENCES

- Anders E., Grevesse N., 1989, *Geochim. Cosmochim. Acta*, 53, 197
- Arnaud K. A., 1996, in *Astronomical Society of the Pacific Conference Series*, Vol. 101, Jacoby G. H., Barnes J., ed, *Astronomical Data Analysis Software and Systems V*, p. 17
- Balucinska-Church M., McCammon D., 1992, *ApJ*, 400, 699
- Birzan L., Rafferty D. A., McNamara B. R., Wise M. W., Nulsen P. E. J., 2004, *ApJ*, 607, 800
- Blanton E. L., Sarazin C. L., McNamara B. R., Clarke T. E., 2004, *ApJ*, 612, 817
- Bohringer H., Voges W., Fabian A. C., Edge A. C., Neumann D. M., 1993, *MNRAS*, 264, L25
- Churazov E., Forman W., Jones C., Böhringer H., 2003, *ApJ*, 590, 225

- Conselice C. J., Gallagher J. S., III, Wyse R. F. G., 2001, *AJ*, 122, 2281
- David L. P., Nulsen P. E. J., McNamara B. R., Forman W., Jones C., Ponman T., Robertson B., Wise M., 2001, *ApJ*, 557, 546
- Dunn R. J. H., Fabian A. C., 2006, *MNRAS*, 373, 959
- Edge A. C., Frayer D. T., 2003, *ApJ*, 594, L13
- Ettori S., Fabian A. C., 2000, *MNRAS*, 317, L57
- Fabian A. C., 1994, *ARA&A*, 32, 277
- Fabian A. C., Sanders J. S., Allen S. W., Crawford C. S., Iwasawa K., Johnstone R. M., Schmidt R. W., Taylor G. B., 2003, *MNRAS*, 344, L43
- Fabian A. C. et al., 2000, *MNRAS*, 318, L65
- Fabian A. C., Sanders J. S., Taylor G. B., Allen S. W., Crawford C. S., Johnstone R. M., Iwasawa K., 2006, *MNRAS*, 366, 417
- Forman W. et al., 2005, *ApJ*, 635, 894
- Graham J., Fabian A. C., Sanders J. S., 2008, *MNRAS*, 349
- Hicks A. K., Mushotzky R., 2005, *ApJ*, 635, L9
- Johnstone R. M., Fabian A. C., Morris R. G., Taylor G. B., 2005, *MNRAS*, 356, 237
- Johnstone R. M., Fabian A. C., Nulsen P. E. J., 1987, *MNRAS*, 224, 75
- Jones C., Forman W., 1999, *ApJ*, 511, 65
- Kaastra J. S., 1992, in *Internal SRON-Leiden Report*, updated version 2.0
- Kaastra J. S. et al., 2004, *A&A*, 413, 415
- Kalberla P. M. W., Burton W. B., Hartmann D., Arnal E. M., Bajaja E., Morras R., Pöppel W. G. L., 2005, *A&A*, 440, 775
- Kriss G. A., Cioffi D. F., Canizares C. R., 1983, *ApJ*, 272, 439
- Liedahl D. A., Osterheld A. L., Goldstein W. H., 1995, *ApJ*, 438, L115
- McNamara B. R., Nulsen P. E. J., 2007, *ARA&A*, 45, 117
- McNamara B. R. et al., 2006, *ApJ*, 648, 164
- McNamara B. R. et al., 2000, *ApJ*, 534, L135
- Mewe R., Gronenschild E. H. B. M., van den Oord G. H. J., 1985, *A&AS*, 62, 197
- Mewe R., Lemen J. R., van den Oord G. H. J., 1986, *A&AS*, 65, 511
- Nulsen P. E. J., Bohringer H., 1995, *MNRAS*, 274, 1093
- Nulsen P. E. J., David L. P., McNamara B. R., Jones C., Forman W. R., Wise M., 2002, *ApJ*, 568, 163
- Nulsen P. E. J., McNamara B. R., Wise M. W., David L. P., 2005, *ApJ*, 628, 629
- O'Dea C. P. et al., 2008, *astro-ph/0803.1772*
- Peterson J. R., Fabian A. C., 2006, *Phys. Rep.*, 427, 1
- Peterson J. R., Kahn S. M., Paerels F. B. S., Kaastra J. S., Tamura T., Bleeker J. A. M., Ferrigno C., Jernigan J. G., 2003, *ApJ*, 590, 207
- Rafferty D. A., McNamara B. R., Nulsen P. E. J., Wise M. W., 2006, *ApJ*, 652, 216
- Salomé P. et al., 2006, *A&A*, 454, 437
- Sanders J. S., Fabian A. C., 2007, *MNRAS*, 381, 1381
- Sanders J. S., Fabian A. C., Allen S. W., Schmidt R. W., 2004, *MNRAS*, 349, 952
- Vikhlinin A., Markevitch M., Murray S. S., 2001, *ApJ*, 551, 160
- Wise M. W., McNamara B. R., Nulsen P. E. J., Houck J. C., David L. P., 2007, *ApJ*, 659, 1153